Mon. Not. R. Astron. Soc. **000**, 1–10 (2004) Printed 7 September 2004 (MN LaTeX style file v2.2)

Near-infrared imaging observations of the southern massive star-forming region G333.6−0.2

Takuya Fujiyoshi,[1,2]⋆ Craig H. Smith,[3]⋆ Toby J. T. Moore,[4]⋆
Stuart L. Lumsden,[5]⋆ David K. Aitken[6]⋆ and Patrick F. Roche[7]⋆

[1]*Subaru Telescope, National Astronomical Observatory of Japan, 650 North A'ohoku Place, Hilo, Hawaii 96720, U.S.A.*
[2]*Department of Physics, University College, University of New South Wales, Australian Defence Force Academy, Canberra ACT 2600, Australia*
[3]*Electro Optic Systems Pty Limited, 55A Monaro Street, Queanbeyan NSW 2620, Australia*
[4]*Astrophysics Research Institute, Liverpool John Moores University, Twelve Quays House, Egerton Wharf, Birkenhead CH41 1LD*
[5]*Department of Physics and Astronomy, University of Leeds, Leeds LS2 9JT*
[6]*Department of Physical Sciences, University of Hertfordshire, Hatfield, HERTS AL10 9AB*
[7]*Astrophysics, Department of Physics, Oxford University, Keble Road, Oxford OX1 3RH*

It will be submitted soon and hopefully accepted soon after that...

ABSTRACT

We present near-infrared broadband JHK' images of the southern massive star-forming region G333.6−0.2. The slope of K-luminosity function towards the region (0.24 ± 0.01) is considered to be equivalent to that expected for main-sequence stars in the solar neighbourhood. Point sources with their $(H - K)$ colour greater than 1 are more likely to be located in extended emission and it is suggested that these objects are physically associated with the H II region.

Key words: H II regions – ISM : individual : G333.6−0.2 – infrared : ISM

1 INTRODUCTION

G333.6−0.2 is one of the brightest compact H II regions in the southern sky (e.g. Becklin et al. 1973; Hyland et al. 1980; Fujiyoshi et al. 1998, 2001, hereafter Paper 1 and Paper 2, respectively). K-band spectroscopy (Wynn-Williams et al. 1978; Moneti & Moorwood 1989) revealed strong emission lines of 2.06-μm He I and 2.17-μm Brγ. Wynn-Williams et al. detected spatial variations in the equivalent widths of these lines, which they attributed to the presence of hot (at more than 600 K) dust grains. Mid-infrared (MIR) spectroscopy (Aitken & Jones 1974; Smith et al. 2000; Paper 2) generally showed flat spectra produced by self-absorption of silicates. Diffraction-limited 12.8-μm [Ne II] image (Paper 1) uncovered a central dip which was interpreted as the ionisation structure of the H II region. The size of the dip was found to be comparable to that of the Ne III ionisation boundary and it was concluded in Paper 1 that the ionising source in G333.6−0.2 is likely to be a cluster of O and B stars, rather than a single star.

It has been shown that direct imaging of star-forming regions in the standard near-infrared (NIR) bands J (1.25 μm), H (1.65 μm), and K (2.2 μm) using infrared (IR) arrays can provide useful information (see e.g. Gatley et al. 1991). By assigning colour terms to sources in the multi-colour images, nearby back- and foreground stars can be discriminated based on their colours. Colour terms can also provide valuable information on the characteristics of young stellar objects (YSOs, C. Lada et al. 1991; Gatley et al. 1991; Lada & Adams 1992).

We have thus applied the direct NIR imaging technique to G333.6−0.2, in order to investigate the nature of newly formed stars in the massive star-forming region. In this paper, we present results from these observations and discuss characteristics of the sources found in this powerful H II region.

2 OBSERVATIONS AND DATA REDUCTION

Table 1 summarises the NIR observations of G333.6−0.2. All measurements were obtained using the IR imager and spectrometer IRIS at the $f/36$ Cassegrain focus of the 3.9-m Anglo-Australian Telescope (AAT), Siding Spring, Australia. The detector element of IRIS is a Rockwell 128×128 HgCdTe NICMOS2 array, which is housed in a closed-cycle compressed helium refrigeration unit. In the imaging mode, wavelength selection is provided by discrete filters such as 'standard' NIR broadband (J, H, K). A more complete de-

⋆ E-mail: tak@subaru.naoj.org (TF); csmith@eostech.com (CHS); tjtm@astro.livjm.ac.uk (TJTM); sll@ast.leeds.ac.uk (SLL); dka@star.herts.ac.uk (DKA); pfr@astro.ox.ac.uk (PFR)

© 2004 RAS

Table 1. Summary of NIR observations of G333.6−0.2.

Date	Filter	λ_0 (µm)	$\Delta\lambda$ (µm)	Integration (sec/position)
27 July 1991	J	1.25	0.25	30 × 3.0
	H	1.65	0.27	30 × 1.5
	K'	2.1	0.35	30 × 1.5

scription of the instrument can be found in Allen et al. (1993).

Images were taken in WIDE mode, which gave a pixel scale of $\sim 0.79 \times 0.79$ arcsec^2. With each filter, a measurement was first obtained with the MIR source (Paper 1) centred in the array, then several offsets were made so as to construct a 3×3 mosaic, resulting in an area coverage of $\sim 4 \times 4$ arcmin^2 because of the overlapping regions.

The images were reduced in a standard manner, consisting of bias and dark frame subtractions and flat-fielding. The subsequent analysis of the reduced broadband images was carried out using the crowded-field photometry software package DAOPHOT (Stetson 1987) within IRAF[1]. Flux calibration was obtained against observations of the standard star HD147778 (J = 8.453, H = 8.151, K = 8.088, Carter & Meadows 1995). Observed apparent K' magnitude $m_{K'}$ was converted to apparent K magnitude m_K, using the empirical relationship (c.f. Bessell & Brett 1988; Wainscoat & Cowie 1992)

$$m_K = m_{K'} - 0.23(H - K').$$

Seeing measured from field stars in the frame (i.e. at NIR wavelengths and the plate-scale) was about 1.6 arcsec.

3 RESULTS AND DISCUSSION

Figure 1 shows the JHK' composite false colour image of G333.6−0.2 (blue = J, green = H, red = K'). The contrast is set so as to emphasize the extended emission which extends almost to the edges of the image. The morphology of the nebulosity is quite complex. The strong emission is concentrated within the central $\sim 1.5 \times 1.5$ arcmin^2. The main nebulosity, with the MIR source at its centre, extends ∼80 arcsec with an extension to the east. Caswell (1997) observed the 6.035-GHz OH maser emission associated with G333.6−0.2. The site of the maser emission, about 20 arcsec east and 5 arcsec north of the main MIR peak, lies in this eastern extension. Generally masers are found offset from the centre of H II regions (e.g. Gaume & Mutel 1987; Caswell 1997) and IR radiation is thought to be one of their plausible pumping mechanisms (e.g. Moore, Cohen & Mountain 1988).

Another interesting morphological feature is the faint extended emission outside the strong central nebulosity and the eastern extension resembling flower petals centred on the MIR source. Some are bead-like fragments, each about 40 arcsec in diameter, and are placed roughly equidistant (∼80 arcsec) from the central IR source making an arc that extends from north-west to almost due south of the main peak. There is a clear gap between the central nebulosity plus eastern extension and the outer fragments, and there are even some thin streamer-like structures running from the centre to the outer nebulosity, strengthening the aforementioned impression of flower petals.

The almost symmetric appearance of petals around the main exciting source possibly suggests a reflection nebulosity. However, the 2-µm imaging polarimetry presented in Paper 2 does not show the centro-symmetric pattern usually observed for polarization produced by scattered light. Instead the pattern implies a dichroic absorption due to magnetically aligned dust grains. Therefore, the nebulosity observed, at least in the inner 30×7.5 arcsec^2 (the field of view of Figure 4 in Paper 2), is not produced by reflection. It can not be ruled out that reflection takes place much further out from the central source, however, as significant absorption is observed in the central region (hence the polarization) it is unlikely that it is the reflection of light from the central source.

[1] IRAF is distributed by the National Optical Astronomy Observatories, which are operated by the Association of Universities for Research in Astronomy, Inc., under cooperative agreement with the National Science Foundation.

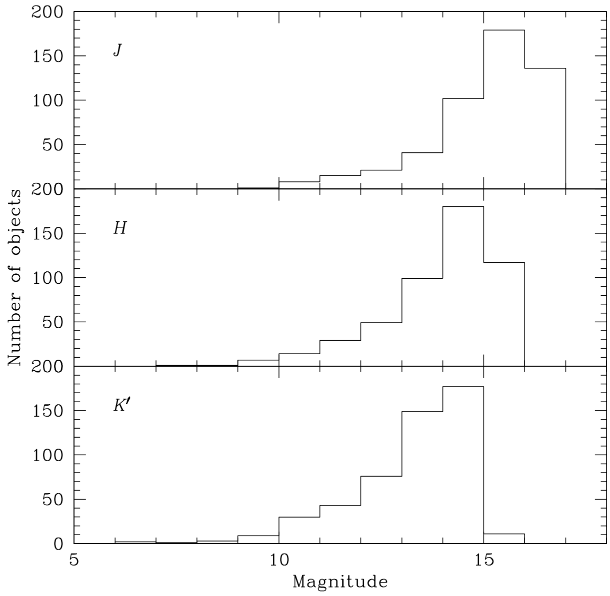

Figure 2. Histogram of all point sources detected in each NIR broadband mosaiced image. The figures shown are, from top to bottom, the histograms for the J, H, and K' images.

3.1 Detection limit

When running DAOPHOT, we set an arbitrary detection threshold of 4 σ. Although the actual σ values were different in each frame, DAOPHOT found ∼500 point sources in each image. Figure 2 shows histogram of all the objects found by DAOPHOT in the JHK' images. The peak in each histogram marks the limit of detection of the current investigation. The 4-σ detection limit of the observations presented here is for $J \sim 16$, $H \sim 15$ and for $K' \sim 14$.

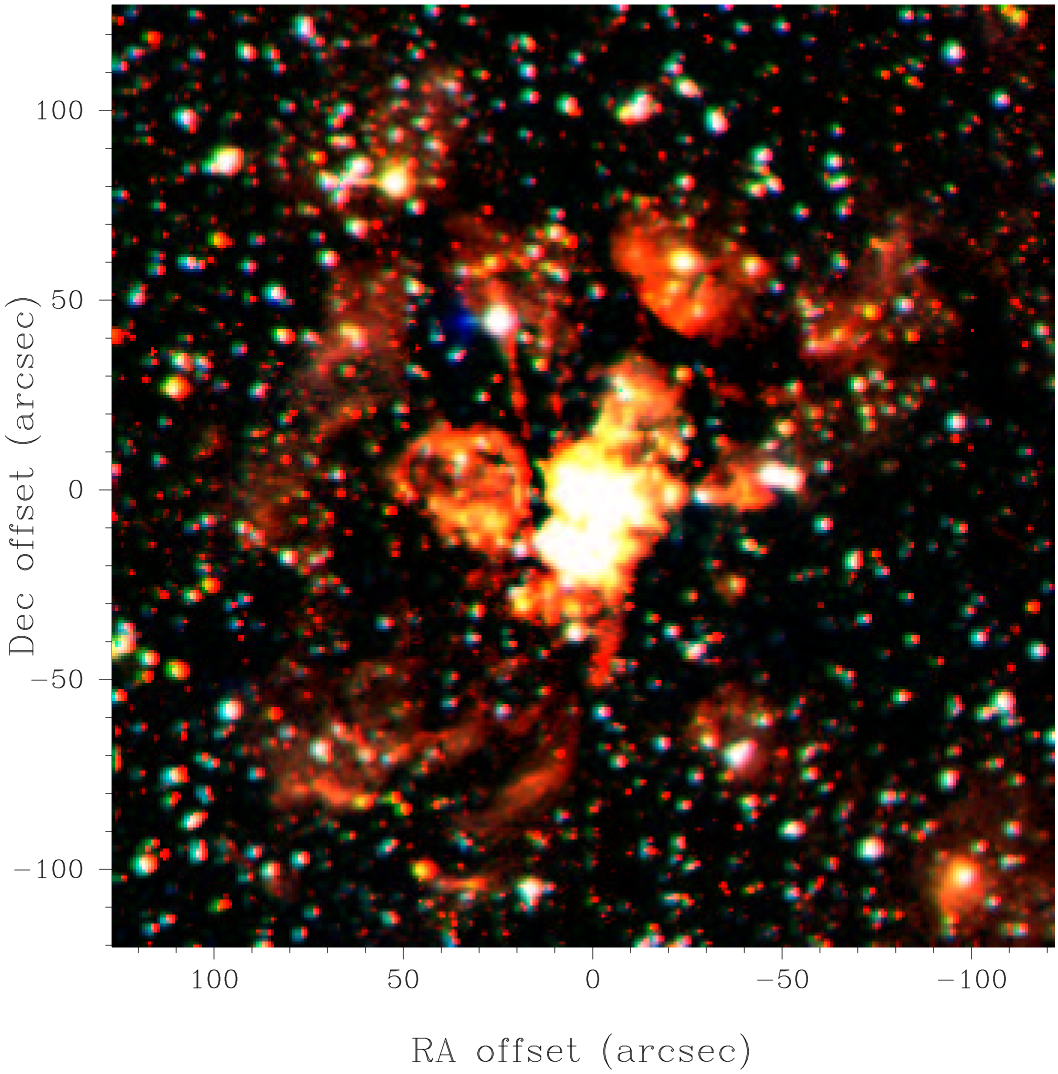

Figure 1. JHK' composite false colour image of G333.6−0.2 (blue = J, green = H, red = K'). Coordinates of the origin are those of the MIR peak (Paper 1), which are RA = $16^{\rm h}22^{\rm m}09\overset{\rm s}{.}6$ and Dec = $-50°06'00''$ (J2000).

3.2 The K-luminosity function

A point source was considered common in all three frames if it was found to have coordinates within 3 pixels (∼2.4 arcsec or about 50 per cent larger than the seeing) of each other in the JHK' images. The somewhat generous tolerance was given in order to allow for the possible shifts between images (although this was corrected beforehand), seeing fluctuations, misregistrations, etc. DAOPHOT in this way recovered ∼300 objects common in all three J, H and K' passbands.

A quick consistency check was performed for a number of brighter objects against 2MASS point source catalogue (PSC), which, although surveyed at a lower spatial resolution than our current study (2MASS used 1.3-m telescopes), has similar limiting magnitudes. After correcting the known colour differences between 2MASS and AAO passbands (Carpenter 2001), it was found that, within each other's uncertainties, our measurements and those of 2MASS are consistent.

For early main-sequence (MS) stars, the K passband occupies the region of the spectrum where the Rayleigh-Jeans approximation holds, under which the observed luminosity is linearly dependent on stellar radius (R_*) and temperature (T_*). For the MS stars, there is a simple power law that relates the stellar mass (m_*) to the radius and temperature ($R_* \sim m_*^{0.8}$, $T_* \sim m_*^{0.4}$; Gatley et al. 1991). In other words, a K-luminosity function (KLF) represents an initial mass function (IMF) in massive star-forming regions.

However, there are two possible causes that may skew the true IMF in the star-forming region. Firstly, it is plausible that some objects are foreground objects (background sources are of little concern as they experience heavy extinction and hence contribute much less to the contamination). 2MASS data were again used to correct this effect. From the PSC, stars with the detection criteria similar to ours (i.e. detected in all three bands with a reasonably high signal-to-noise ratio, etc.) were selected in the same field-of-view as our current study ($\sim 4\times4$ arcmin^2) at $l = 333.0°, b = -0.2°$. The 2MASS Ks magnitudes were then transformed into the AAO K and finally the number of stars in each magnitude

© 2004 RAS, MNRAS **000**, 1–10

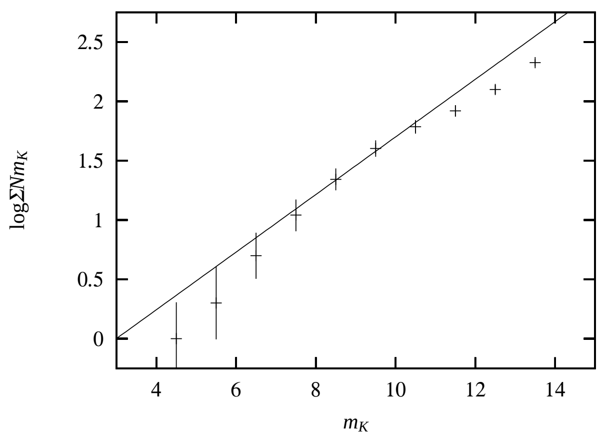

Figure 3. The cumulative K-luminosity function for the common point sources ($m_K < 14$) found in the JHK' mosaiced frames. The errorbars represent the square-root of the number of sources in each bin.

interval was adjusted for these field stars. Secondly, the foreground extinction may also affect the KLF. As there is a possibility that the extinction varies across the face of the H II region (see later), the extinction encountered by each source at K is estimated via $A_K \sim 0.85(J - H)$ (Martin & Whittet 1990).

Figure 3 shows the cumulative KLF after applying these two corrections. The straight line represents the best fit to the data, which has the slope of 0.24 ± 0.01. This is similar to, but slightly smaller than, the value expected for the Salpeter (1955) IMF of 0.26. It is noted, however, that our method of studying only the stars detected in all three bands, while highly beneficial in many other instances (e.g. warrants against spurious detections, provides colour terms to each source and in the above case the extinction, etc.), may be slightly biased towards bright objects. That is, stars may have to be relatively bright to be detected in the more heavily extinguished J-band, as well as at H and K, resulting in an overabundance of bright objects and under-representation of fainter stars in the KLF. Taking into account such a possibility, the KLF in G333.6−0.2 is considered to be equivalent to that derived for local stars by Salpeter (1955).

DePoy et al. (1990) found a similar result (a KLF slope ~ 0.26) in NGC 2023, as did C. Lada et al. (1991) in M17. E. Lada et al. (1991) and Lada, Young & Greene (1993) have pointed out that, in high-mass star-forming regions, newly formed stars should possess almost MS luminosities even in their pre-MS phase, and so the KLF would display a similar form to that of the local field star population. It is perhaps not surprising then that G333.6−0.2, too, shows such a luminosity function.

3.3 Colour-magnitude diagram

Figure 4 shows the $(H - K)$ colour versus the apparent K magnitude m_K, colour-magnitude (C–M) diagram. The locus expected for MS stars is also drawn using the absolute visual magnitudes of MS stars tabulated in Lang (1992) and the intrinsic $(V - K)$ colours of MS stars from Koornneef (1983). These values were then scaled to the distance of 3.0 kpc (an assumed distance to G333.6−0.2, Colgan et al. 1993). The NIR extinction law of Martin & Whittet (1990) [$(H-K) = 0.062A_V$, where $A_V = \frac{A_K}{0.092}$] is drawn from each MS spectral type and the loci of MS stars are redrawn at $A_V = 5$, 10,...,40, as indicated.

Landini et al. (1984) found the NIR extinction towards G333.6−0.2 can be described well by a power law of the form $A_\lambda \propto \lambda^{1.85\pm0.05}$. Martin & Whittet (1990) derived a mean NIR extinction curve from a compilation of a large number of previously published data and found the power index to be identical to that of Landini et al.'s within the uncertainty (1.84 ± 0.03).

The faint-end (lower-end) of the diagram is bounded by the 4-σ detection limit of the current study, which is marked by the dashed line. There is a concentration of data points located between this line, the extinction curve from spectral type B3 and the $(H - K)$ values 0 to 1. In fact, almost 70 per cent of the sources (215 out of 315) belongs to this group. These objects generally exhibit very low to moderate extinction ($A_V < 15$) and are relatively faint. They appear to suffer normal interstellar extinction often encountered by stars in and/or behind a dark cloud (e.g. Teixeira & Emerson 1999), although some are probably foreground field stars. Extinction towards the central region of G333.6−0.2 is estimated to be $A_V \sim 20$ (Rank et al. 1978). The stellar spectral types later than B3 rule them out from being the exciting sources for the H II region. The point sources in this category [stellar spectral type later than B3 and $(H-K) < 1$] also do not show significant IR excess, which implies that they are probably more evolved and not cocooned in circumstellar materials. YSOs generally exhibit significant IR excess due to the presence of circumstellar dust (e.g. Lada & Adams 1992).

An interesting trend in Figure 4 is that the brighter the point source the more IR excess it exhibits. For example, most objects earlier than stellar spectral type O6 show $(H - K) > 1$. Although it is not possible to distinguish heavy extinction from IR excess and to establish the nature of these sources with the information presented in the C–M diagram alone, as it will become apparent later on, these objects are very likely to be physically associated with the H II region and therefore to possess intrinsic IR excess.

The obvious standouts in Figure 4 are the three data points in the top-right-hand corner of the diagram. They all have $H - K$ colour of more than 3 and are all brighter than $m_K = 8$. For example, the apparent K magnitude of the brightest of the three, which happens to be the brightest of all the common point sources, is $m_K \approx 5.8$. Ignoring interstellar extinction, this translates to the absolute K magnitude $M_K \approx -6.6$. Such brightness is thought to be more appropriate for supergiants rather than for the MS stars (Schaerer et al. 1996).

Comparison with the MIR images (Paper 1) reveals that the position of the brightest source coincides (within an arcsec) with the MIR main peak, making it an obvious candidate for the NIR counterpart of the MIR source. In other words, it is located at the centre of the intense nebulosity and this may offer a plausible explanation for its strong apparent brightness at K and the large $(H - K)$ colour excess.

In an H II region, there are a number of contributions to the total flux in the K-band other than from bound-free (b–f) and free-free (f–f) emissions, and the stellar continuum

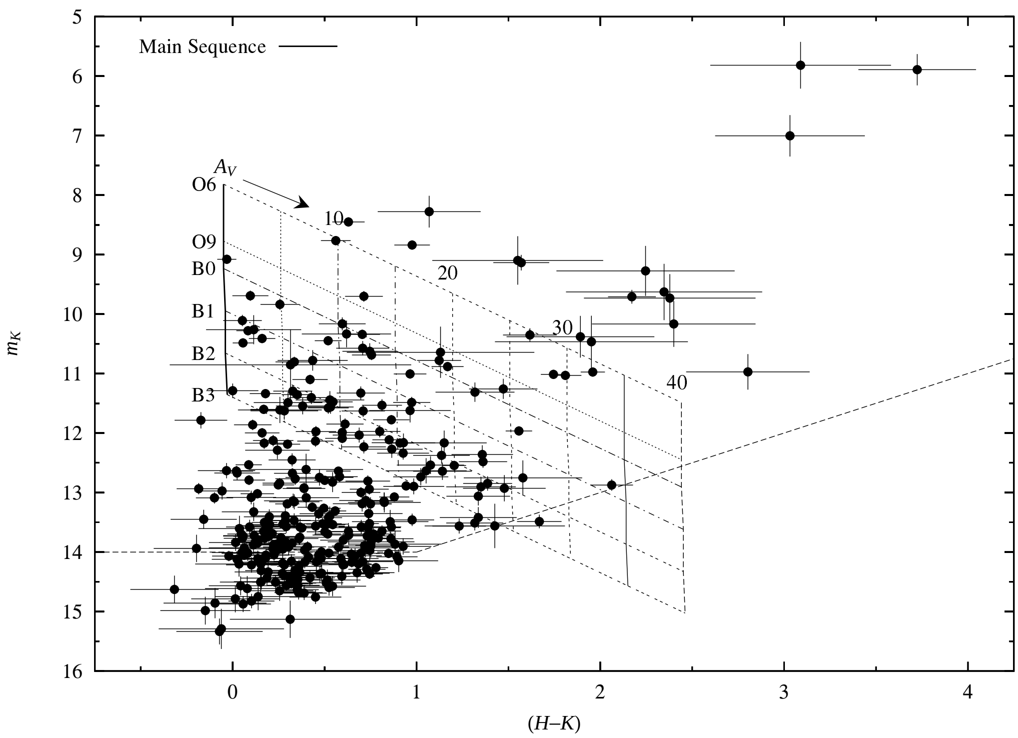

Figure 4. The colour-magnitude diagram: A diagram of the $(H-K)$ colour versus apparent K magnitude, m_K, constructed for the common point sources in G333.6−0.2. Also drawn are the locus expected for the main-sequence stars and its positions at various visual extinctions as indicated (see text for detail). The dashed line at the lower-end (faint-end) bounds the 4-σ detection limit of the current study (i.e. $m_K \sim 14$ and $m_H \sim 15$).

itself. For example, Wynn-Williams et al. (1978) estimated that emission from hot dust grains (at a temperature in excess of 600 K) is important in the 2-μm band in the central region of G333.6−0.2. Assuming there is no thermal emission at J, and the stellar radiation is on the Rayleigh-Jeans tail ($F_* \propto \lambda^{-4}$), the dust contribution to the total flux at H and K were estimated for the three bright objects in the top-right-hand corner of the C–M diagram. These values were then compared with those determined from a simple grey-body (emissivity index $\alpha = 1.5$) emission at 600 K. The results are consistent with one another and indicate that the dust contribution at K is an order of magnitude greater than that at H.

This implies that, for intrinsically red objects in the K-band, the stellar radiation is superposed on top of the thermal emission from hot dust and photometry performed on such a structure would lead to an overestimate of stellar flux in the star. In fact, the three objects at the top-right-hand corner of the C–M diagram have the three brightest apparent K magnitudes and are all located in the intense central nebulosity of G333.6−0.2. Therefore, their apparent K magnitudes and the $(H-K)$ colours are unlikely to represent their true stellar values. Again comparison with the MIR continuum image (Figure 2, Paper 1) reveals that the location of the third brightest source coincides within 1 arcsec with that of the secondary MIR peak 4 arcsec to the east of the main peak. With such prominent MIR counterparts, they (the brightest and third brightest sources) are most probably physically associated with the H II region with significant amount of warm gas and dust surrounding these objects. However, the second brightest source, which in fact has the largest $(H-K)$ colour, does not have an obvious MIR counterpart. It is instead located in an extension south-west of the main peak (described as the south-west extension in Paper 1. See also Figure 7 below).

3.4 Colour-colour diagram

Figure 5 shows the $(H-K)$ colour versus $(J-H)$ colour, colour-colour diagram for the common objects found in G333.6−0.2. The colours of MS stars and those of giant stars were taken from Koornneef (1983). The two dashed lines again represent the Martin & Whittet (1990) IR extinction law $[(J-H) \sim 1.7(H-K)]$. So the area between these extinction curves is where MS/giant stars that suffer extinction according to the mean interstellar extinction law derived by Martin & Whittet should lie.

Sources that are later than the stellar spectral type B3 and exhibit $(H-K) < 1$ in the C–M diagram (Figure 4) are represented by open circles. The rest of the point sources are drawn with filled circles. It is immediately obvious that open circles are all concentrated along the two parallel IR extinction curves and implied visual extinction to them is less than ∼15, just as seen earlier in the C–M diagram. Most data points with $(H-K) < 1$, both open and filled circles, seem to lie along the extinction curves and only when the $(H-K)$ colour exceeds 1, the point sources start exhibiting appreciable amount of deviation from the curves.

Since such a large fraction (more than 80 per cent) of the point sources in the field studied appears to follow the mean

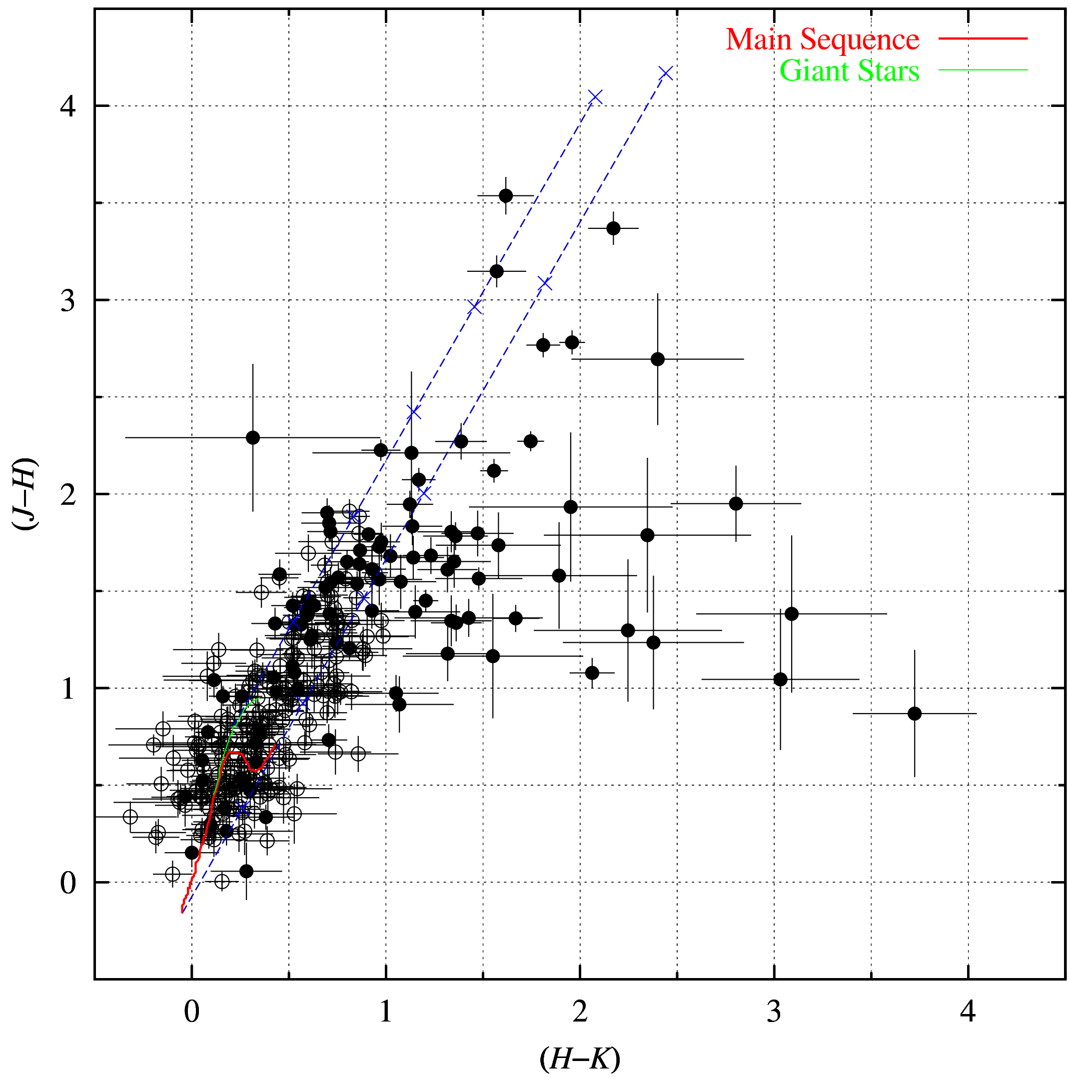

Figure 5. The colour-colour diagram: A diagram of the $(H - K)$ colour versus the $(J - H)$ colour constructed for the common sources in G333.6−0.2. *Open circles*: Sources that are later than the stellar spectral type B3 and have $(H - K) < 1$ (see Figure 4). *Filled circles*: the rest of the common point sources [i.e. those which are earlier than B3 and have $(H - K) > 1$]. Also drawn are the loci expected for the main-sequence and giant stars. The dashed parallel lines are the interstellar IR extinction curve of Martin & Whittet (1990). Crosses are drawn at A_V = 5, 10, 15, 20 and 30 (and at 40 for the lower curve).

IR extinction law derived by Martin & Whittet (1990), it is likely that those that do not do so have intrinsic IR excess, rather than exhibiting peculiar extinction. There is, however, one data point above the extinction curves (although it has rather large errorbars and hence only one sigma away from the curves). Again it is very unlikely that there is a special extinction law only towards this one source but rather that this data point is in fact spurious. Identification of the source position reveals that this source is located in a relatively strong extended nebulosity and positions between individual frames shift by more than 2 pixels. Considering these facts, it is most likely that this source is just a knot in the extended emission. It is quite remarkable that only one such a source was picked up by DAOPHOT and this result essentially justifies the generous positional tolerance (3 pixels) given in finding the common point sources in the three frames. It also demonstrates the benefit of having three filters and selecting only common sources found in all the bands for further studies as it tends to warrant against supurious detections (recall that, of the ∼500 potential point sources detected in each frame, ∼200 have been rejected). Figure 6 illustrates the spatial distribution of the common objects with different $(H - K)$ colours. The sources with $(H - K) > 1$ show a strong tendency to be found in areas where extended nebulosity is also present.

Although many sources with $(H - K) > 1$ have rather large uncertainties, in most cases the lower limits clearly exceed $(H - K) = 1$ (see Figures 4 & 5). There are several possible causes for the large uncertainties. The most obvious being the difficulty in extracting accurate photometry in the presence of strongly varying background (i.e. the complex extended nebulosity), and the finite spatial resolution of the current study may also contribute (i.e. some objects could be unresolved binaries or multiples, which would result in poorer point-spread function fits in DAOPHOT).

In order to confirm/dismiss the validity of the

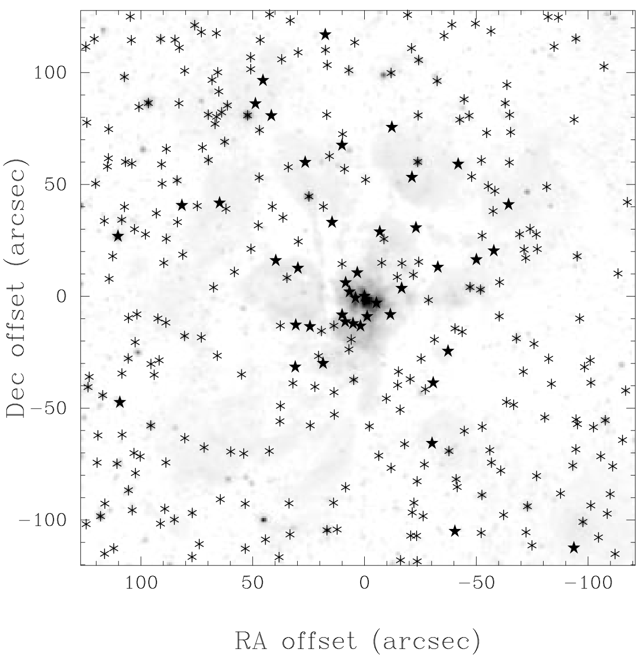

Figure 6. Spatial distribution of the common objects. ⋆ represents point sources with $(H-K) > 1$ and $*$ the rest [i.e. those with $(H-K) < 1$]. Superposed on the grey-scale K' image.

DAOPHOT results, a simple test was performed. A couple of artificial point sources of known magnitudes (one reasonably bright and another faint) were added inside a relatively strong extended emission in the K' frame. When DAOPHOT was run again with these additional point sources it recovered the correct magnitudes within the empirical uncertainty measured by the software verifying the validity of the results. Also, another consistency check was carried out against the 2MASS PSC for a number of objects with $(H-K) > 1$, and again it was confirmed that our measurements and those of 2MASS agree within each other's uncertainties.

Given these considerations, it is most likely that sources with $(H-K) > 1$ are physically associated with the nebulosity and their large IR excesses are intrinsic to these objects. The most plausible scenario is then that they are embedded inside a considerable amount of dust and gas and that they are the heat sources for the H II region.

We have suggested in the previous section that hot dust is important in causing the substantial excess emission at 2 µm. Indeed, blackbodies at about 1,000 K would radiate significantly in the K-band. Dust grains must be close to the heat sources to attain such high temperatures (near dust sublimation temperatures). For late O to early B stars, the sublimation radius is of the order of a few tens of aus (e.g. Osorio, Lizano & D'Alessio 1999; Monnier & Millan-Gabet 2002). How the material accumulates onto a forming massive protostar is very poorly understood at present. Nonetheless, accretion onto massive stars is believed to become more difficult as the stellar mass increases because of the strong radiation pressure from the central star, and faster stellar winds from such stars are also thought to impede the further accretion (Stahler, Palla & Ho 2000). Adams (1993) suggested that in order to overcome these difficulties, accretion via a circumstellar disc is perhaps necessary in forming massive stars. In any case, the need to transfer angular momentum is expected to lead to flattening of the infalling envelope and possibly to the formation of a circumstellar disc. The implication may be the excess IR emission originates in the vicinity of the newly formed massive stars and those circumstellar materials could be in the form of discs.

There have been detections of shock-excited molecular line emission towards G333.6-0.2 [the 2.12-µm $v = 1-0$ S(1) H_2 by Storey (1983) and Moneti & Moorwood (1989), and the 163-µm CO ($J = 16-15$), etc., by Storey et al. (1989)]. Moreover, Juvela (1996) observed the 2.6-mm CO ($J = 1-0$) line profile indicative of the presence of high-velocity molecular gas. One plausible mechanism for exciting/driving these molecules is the star/disc accretion/outflow system and this could be taken as further evidence of the possible existence of circumstellar discs in G333.6−0.2. However, it should be noted that they could also be caused by stellar wind from newly formed massive stars and the expanding H II region pushing the surrounding molecular cloud [see Hofmann, Larson & Fink (1986) for an implication of stellar wind in G333.6−0.2, and Fujiyoshi (1999, also Fujiyoshi et al., in preparation) for a likely manifestation of ionised outflows].

3.5 Morphology

The flower petal-like morphology seen in the three-colour JHK' image (Figure 1. See also Figure 6) discussed earlier and absence of nebulosity between the central extended emission and petals may result from higher extinction. In fact, the gap ∼16 arcsec east of the main IR source and the neighbouring extended emission further east is likely to be due to high extinction (Fujiyoshi et al., in preparation). There are also no common point sources found by DAOPHOT in this narrow gap (see Figure 6). Indeed, there appears to be a reduction in the number of point sources detected within the gaps, which is consistent with these regions being more heavily obscured. Few objects there are in the gaps all exhibit $(H-K) < 1$ and tend not to show significant extinction which is indicative of them being foreground field stars. In Figure 6, there is a concentration of sources with $(H-K) > 1$ in and around the central extended emission. This apparent positional association of the point sources having large IR excesses with the extended emission is likely to be caused by the physical association of the embedded or exciting sources with the H II region, as argued above.

Although there are a few exceptions (notably in faint regions in the far-south and far-east of the central IR source. See Figure 6), each extended emission houses at least one object with $(H-K) > 1$. It is possible then that these extended emission regions are quite separate from the central source and are independently excited by those objects found inside the nebulosity. Even in this case heavy extinction can still not be ruled out as the possible mechanism producing the gaps. Sensitive observations at longer wavelengths are required to resolve this issue.

Figure 7 shows the central $\sim 30 \times 30$ arcsec^2 of each frame comprising Figure 1. The overall similarity of these three images not only with one another but also to the MIR continuum image (Figure 2, Paper 1) is quite remark-

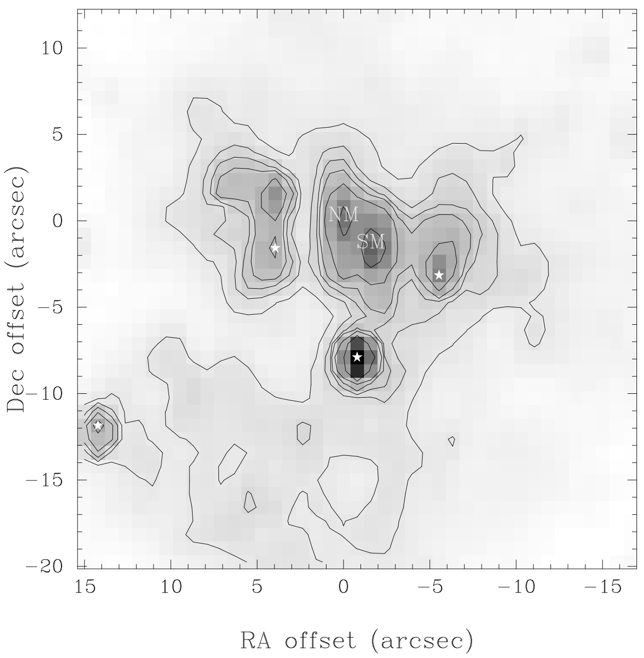

(a) The inner 30 × 30 arcsec^2 of the J image.

Figure 7. A grey-scale image of the inner 30 × 30 arcsec^2 of the mosaiced G333.6−0.2 images. The image is uncalibrated and contours are drawn arbitrary. Point sources NM and SM (see text) are labelled and common point sources easily recognizable by eye are marked with stars. Coordinates of the origin are as in Figure 1.

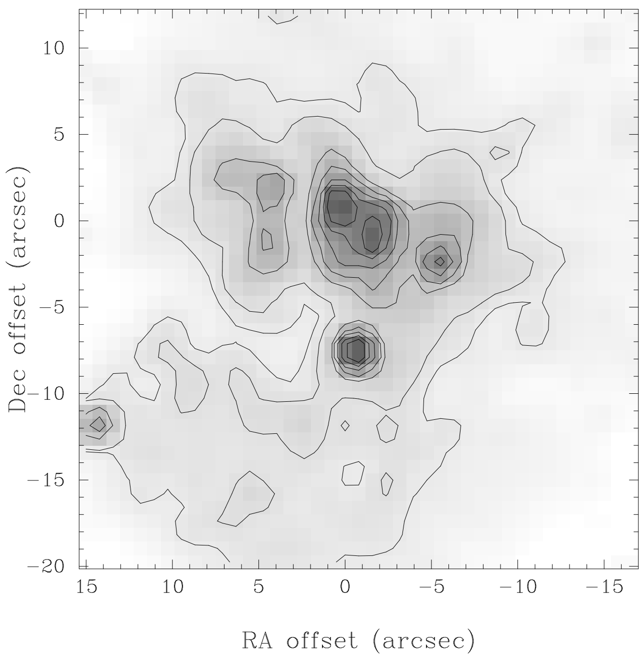

(b) The inner 30 × 30 arcsec^2 of the H image.

Figure 7. Same as (a) but for the H image.

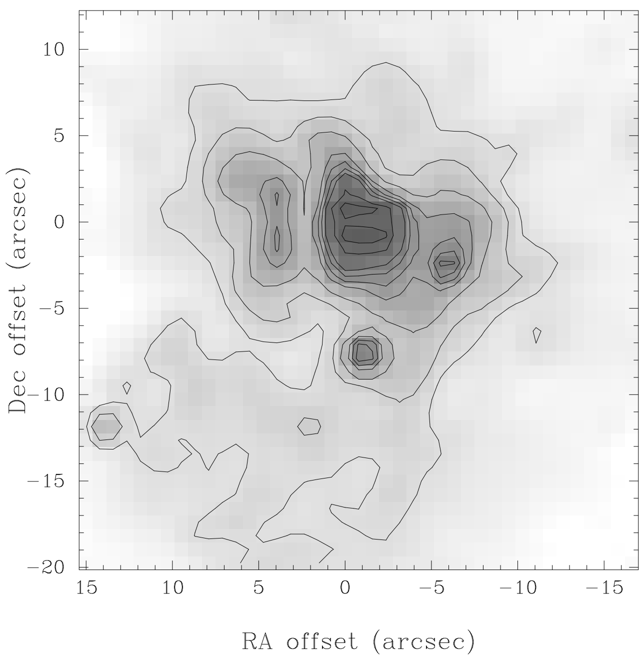

(c) The inner 30 × 30 arcsec^2 of the K' image.

Figure 7. Same as (a) but for the K' image.

able. Similarities include: the slightly north-south elongated, teardrop-shaped central peak with an extension to the west; a north-south gap of emission to the east and further east a north-south elongated secondary peak; a faint tail-like structure arising south of the main peak curling up to the east.

However, since the MIR emission is dominated by thermal radiation from optically thin dust grains while the JHK' fluxes originate largely from stellar radiation and f–f and b–f emissions, they show different features as well as the similarities. For example, there appears to be two sources within the MIR main peak, which are denoted NM (Northern Main) and SM (Southern Main) here. Comparison of the JHK' and MIR continuum images reveals that the position of NM coincides (within ±1 arcsec of each other) with the MIR main peak [RA = $16^{\rm h}22^{\rm m}09\overset{\rm s}{.}6$ and Dec = $-50°06'00''$ (J2000), Paper 1]. Therefore, it is very likely that the main exciting source ionizing this H II region is embedded at this location. However, SM, prominent and point-source like in the J and H images, changes its shape dramatically in the K' frame to a rather smeared, east-west elongated appearance. In fact, probably because of this, DAOPHOT did not recognize SM as a common source. NM too is somewhat elongated east-west at K' and this effect (elongation of these peaks) could have been caused by misregistrations. The position of the MIR secondary peak to the east of the main peak coincides with a common NIR point source.

The bright star ∼8 arcsec south of NM, which is the fourth brightest amongst the common sources and exhibits a moderate IR colour excess [$(H-K)\sim 1$], does not have its counterpart in the MIR images and it could be a nearby field star, or a young star at a more evolved stage that has already shed most of its associated dust. Can objects at different stages of evolution co-exist at such proximity in a star-forming region? In Orion, for example, the bright MIR source IRc2 is totally obscured at NIR wavelengths. The Trapezium OB cluster, more dominant in the visible and NIR, is found relatively nearby. Although the BN-KL complex is thought to be embedded in the OMC-1 molecular cloud, which lies behind the Trapezium OB cluster, the projected distance on the plane of the sky is ∼0.1 pc. This is comparable to the distance between the NM and the source to the south of ∼0.1 pc at 3.0 kpc.

However, the comparison seems to end there. Neither the 12.8-μm [Ne II] image (Paper 1), nor the 3.4-cm radio synthesis map (Fujiyoshi et al., in preparation) shows the presence of hot gas at the position of the star, even though its apparent brightness suggests it should be an ionising source. In fact, this star is also reasonably bright in the visible and is listed in the Guide Star Catalog (S23021018476, $m_V = 13.95 \pm 0.38$, GSC 2.2). So perhaps it is more likely that this star is a bright foreground field star, rather than a *bona fide* member of this star-forming complex. Indeed, when presenting a contour map of the 1-μm CCD image, Geballe et al. (1981) removed the contribution from this star all together, simply dismissing it as a nearby field star.

3.6 Massive star formation in G333.6−0.2

It was found in Paper 1 that, if all the exciting sources were of the same stellar spectral type, about a dozen O8V stars would be required to reproduce the observed Ne III ionisation boundary radius. This number is consistent with that determined from the radio and NIR recombination studies (Fujiyoshi et al., in preparation).

Franco, Shore & Tenorio-Tagle (1994) calculated the massive star formation capacity of molecular clouds and concluded that the maximum number of massive stars that can be formed is about 1 per $10^4\ M_\odot$ of average molecular gas (the hydrogen number density, $n_{\mathrm{H}_2} \sim 10^2\ \mathrm{cm}^{-3}$), or 10 per $10^4\ M_\odot$ of dense molecular gas ($n_{\mathrm{H}_2} \sim 10^3\ \mathrm{cm}^{-3}$). Cheung et al. (1980) mapped G333.6−0.2 at 1 mm with a 1-arcmin resolution and estimated the total gas mass of $1 \times 10^5\ M_\odot$. Storey et al. (1989) observed a number of CO transitions in the far-IR using a 55-arcsec beam and estimated a range of hydrogen density ($\sim 10^{4-5}\ \mathrm{cm}^{-3}$). It is unlikely that such a high density would be found throughout the complex, however, G333.6−0.2 would certainly qualify as a 'dense' cloud. So according to Franco et al.'s calculation, G333.6−0.2 is capable of producing up to 100 OB stars.

The number of stars formed in a molecular cloud is essentially limited by the combined effects of supernovae, stellar winds, and expansion of H II regions, which eventually destroy the reservoir of star-forming materials, i.e. the molecular cloud. Photoionisation is the most efficient mechanism for cloud destruction (e.g. Franco 1993): as OB stars are formed, more H II regions are produced and their expansion is largely responsible for ionizing and photo-dissociating gas, and star formation stops when the entire cloud is ionized. A lower star formation efficiency is expected from the 'blister' erosion (i.e. star formation near or on the boundary of a molecular cloud) as it is the most rapid phase of cloud destruction (Franco et al. 1994). G333.6−0.2 has been found to have a blister geometry viewed face-on (Hyland et al. 1980). Only a fraction of the total mass of the natal molecular cloud is transformed into stars by star formation process and this fraction, or the star formation efficiency, has been found to be rather low (see e.g. Lada, Strom & Myers 1993). The pure blister erosion would result in the final star formation efficiencies between 2 and 10 per cent for average molecular gas (Franco et al. 1994).

Miller & Scalo (1979) derived the IMF in the solar neighbourhood and found that the fraction of mass in the IMF contained in stars more massive than 20 $M_\odot$ (approximately the mass of an O8V star) is about 0.03. The Miller-Scalo IMF shows a reasonable agreement with the Salpeter (1955) IMF, to which the G333.6−0.2 KLF was found to have an equivalent slope (see Section 3.2). A dozen O8V stars in G333.6−0.2 would make up about 300 $M_\odot$ in mass. If this mass represented 3 per cent of the total mass in the Miller & Scalo (1979) IMF, the total mass found in stars in the IMF would be $\sim 10^4\ M_\odot$. This would imply that the star formation efficiency in G333.6−0.2 is ∼10 per cent which is the high-end of the efficiencies quoted for the blister erosion in average molecular clouds by Franco et al. (1994). However, as mentioned earlier, G333.6−0.2 is a dense molecular cloud complex, and the pure blister erosion in the theoretical sense would probably not apply, and so perhaps star formation in G333.6−0.2 has not yet been ceased. In other words, star formation in this H II region is still on-going.

Molecular maser emissions, such as OH and methanol, at radio frequencies are thought to be excellent signposts for sites of massive star formation, which are often heavily obscured by dust (e.g. Kylafis 1991). It is interesting to note that Caswell (1997) only found OH masers associated with G333.6−0.2 but no methanol emission. Recently Walsh et al. (1998) proposed that the methanol masers represent an earlier phase of massive star formation before observable ultracompact (UC) H II regions are formed around massive stars, and as UC H II regions evolve the methanol maser sites are quickly destroyed. Although the non-detection of the methanol masers in G333.6−0.2 could be a geometric effect (i.e. the maser paths may not be facing towards us), together with the observations of the OH masers, it may indicate that the H II region is somewhat older than 10^5 yrs (Cragg, Sobolev & Godfrey 2002). On the other hand, the presence of O8V stars, which excite the H II region, places an upper-limit on its lifetime at $\sim 10^6$ yrs.

4 CONCLUSIONS

The near-infrared J (1.25 μm), H (1.65 μm), and K' (2.1 μm) broadband imaging observations of the bright southern compact H II region G333.6−0.2 are presented. The K-luminosity function (KLF) towards the region studied was constructed. It was found that the slope of the KLF (0.24 ± 0.01) was equivalent to that expected for the local star population. This is probably because G333.6−0.2 is a massive star-forming region and so the newly formed stars in it have already reached luminosities very close to their main sequence values. The JHK colour study of the region showed that point sources with the $(H - K)$ colour greater than 1 tend to be found within the extended nebulosity.

© 2004 RAS, MNRAS **000**, 1–10

This suggested that the colour excess is intrinsic and those sources are most likely to be physically associated with the H II region.

ACKNOWLEDGMENTS

We would like to thank Dr. Michael Burton for obtaining the data presented in this paper as part of the AAT service observations. We would also like to thank the anonymous referee for the valuable comments. This publication makes use of data products from the Two Micron All Sky Survey, which is a joint project of the University of Massachusetts and the Infrared Processing and Analysis Center/California Institute of Technology, funded by the National Aeronautics and Space Administration and the National Science Foundation.

REFERENCES

Adams F. C., 1993, in Cassinelli J. P., Churchwell E. B., eds, ASP conf. Ser. 35, Massive stars: their lives in the interstellar medium. ASP, San Francisco, p. 56
Aitken D. K., Jones B., 1974, MNRAS, 167, 11P
Allen D. A., et al., 1993, PASAu, 10, 298
Becklin E. E., Frogel J. A., Neugebauer G., Persson S. E., Wynn-Williams C. G., 1973, ApJ, 182, L125
Bessell M. S., Brett J. M., 1988, PASP, 100, 1134
Carpenter J. M., 2001, AJ, 121, 2851
Carter B. S., Meadows V. S., 1995, MNRAS, 276, 734
Caswell J. L., 1997, MNRAS, 289, 203
Cheung L. H., Frogel J. A., Gezari D. Y., Hauser M. G., 1980, ApJ, 240, 74
Colgan S. W. J., Haas M. R., Erickson E. F., Rubin R. H., Simpson J. P., Russell R. W., 1993, ApJ, 413, 237
Cragg D. M., Sobolev A. M., Godfrey P. D., 2002, MNRAS, 331, 521
DePoy D. L., Lada E. A., Gatley I., Probst R., 1990, ApJ, 356, L55
Franco J., 1993, RMxAA, 26, 13
Franco J., Shore S. N., Tenorio-Tagle G., 1994, ApJ, 436, 795
Fujiyoshi T., 1999, in Nakamoto T., ed., Star formation 1999. Nobeyama Radio Observatory, p. 401
Fujiyoshi T., Smith C. H., Moore T. J. T., Aitken D. K., Roche P. F., Quinn D. E., 1998, MNRAS, 296, 225 (Paper 1)
Fujiyoshi T., Smith C. H., Wright C. M., Moore T. J. T., Aitken D. K., Roche P. F., 2001, MNRAS, 327, 233 (Paper 2)
Gatley I., Merrill K. M., Fowler A. M., Tamura M., 1991, in Elston R., ed., ASP Conf. Ser. 14, Astrophysics with infrared arrays. ASP, San Francisco, p. 230
Gaume R. A., Mutel R. L., 1987, ApJS, 65, 193
Geballe T. R., Wamsteker W., Danks A. C., Lacy J. H., Beck S. C., 1981, ApJ, 247, 130
Hofmann R., Larson H. P., Fink U., 1986, A&A, 160, 18
Hyland A. R., McGregor P. J., Robinson G., Thomas J. A., Becklin E. E., Gatley I., Werner M. W., 1980, ApJ, 241, 709
Koornneef J., 1983, A&A, 128, 84
Kylafis N. D., 1991, in Lada C. J., Kylafis N. D., eds, The physics of star formation and early stellar evolution. Kluwer, Dordrecht, p. 269
Lada C. J., Adams F. C., 1992, ApJ, 393, 278
Lada C. J., Strom K. M., Myers P. C., 1993, in Levy E. H., Lunine J. I., eds, Protostars and planets III. The University of Arizona Press, p. 245
Lada C. J., Young E. T., Greene T. P., 1993, ApJ, 408, 471
Lada C. J., DePoy D. L., Merrill K. M., Gatley I., 1991, ApJ, 374, 533
Lada E. A., DePoy D. L., Evans N. J., II, Gatley I., ApJ, 1991, 371, 171
Landini M., Natta A., Oliva E., Salinari P., Moorwood A. F. M., 1984, A&A, 134, 284
Lang K. R., 1992, Astrophysical data I. Planets and stars. Springer-Verlag
Martin P. G., Whittet D. C. B., 1990, ApJ, 357, 113
Miller G. E., Scalo J. M., 1979, ApJS, 41, 513
Moneti A., Moorwood A. F. M., 1989, in ESA, Infrared spectroscopy in astronomy. p. 299
Monnier J. D., Millan-Gabet R., 2002, ApJ, 579, 694
Moore T. J. T., Cohen R. J., Mountain C. M., 1988, MNRAS, 231, 887
Osorio M., Lizano S., D'Alessio P., 1999, ApJ, 525, 808
Rank D. M., Dinerstein H. L., Lester D. F., Bregman J. D., Aitken D. K., Jones B., 1978, MNRAS, 185, 179
Salpeter E. E., 1955, ApJ, 121, 161
Schaerer D., de Koter A., Schmutz W., Maeder A., 1996, A&A, 312, 475
Smith C. H., Wright C. M., Aitken D. K., Roche P. F., Hough J. H., 2000, MNRAS, 312, 327
Stahler S. W., Palla F., Ho P. T. P., 2000, in Boss A. P., Russell S. S., eds, Protostars and planets IV. University of Arizona Press, p. 327
Stetson P. B., 1987, PASA, 99, 191
Storey J. W. V., 1983, MNRAS, 202, 105
Storey J. W. V., Harnett J. I., Lugten J. B., Crawford M. K., Stacey G. J., Watson D. M., Genzel R., 1989, MNRAS, 237, 1001
Teixeria T. C., Emerson J. P., 1999, A&A, 351, 303
Wainscoat R. J., Cowie L. L., 1992, AJ, 103, 332
Walsh A. J., Burton M. G., Hyland A. R., Robinson G., 1998, MNRAS, 301, 640
Wynn-Williams C. G., Becklin E. E., Matthews K., Neugebauer G., 1978, MNRAS, 183, 237